



Geometric effects of nanocrystals in nonvolatile memory using block copolymer nanotemplate

Jong-Won Lee^a, Seong-Wan Ryu^{a,*}, Dong Ok Shin^b, **Bong Hoon Kim^b**, Sang Ouk Kim^b, Yang-Kyu Choi^{a,1}

^aSchool of Electrical Engineering and Computer Science, Department of Electrical Engineering, KAIST, 373-1 Guseong-dong, Yuseong-gu, Daejeon 305-701, Republic of Korea

^bDepartment of Materials Science and Engineering, KAIST Institute for the Nanocentury, 373-1 Guseong-dong, Yuseong-gu, Daejeon 305-701, Republic of Korea

ARTICLE INFO

Article history:

Received 7 November 2008

Received in revised form 11 March 2009

Accepted 13 March 2009

Available online 5 May 2009

The review of this paper was arranged by Prof. A. Zaslavsky

Keywords:

Nonvolatile memories (NVM)

Nanocrystal (NC)

Geometric effect

Block copolymer (BCP) nanotemplate

Modeling

Capacitive-coupling ratio

ABSTRACT

This study describes geometric characteristics of a nonvolatile memory (NVM) device with a designed chromium (Cr) nanocrystal (NC) floating gate. By using a block copolymer (BCP) nanotemplate as a mask layer, cone-shaped NCs and disc-shaped NCs were formed. It was found that the NVM device using the cone-shaped NC had a better program efficiency than that of the device using the disc-shaped one. This trend was verified by a theoretical model, which considered an effect of the capacitive-coupling ratio between a control gate and a NC floating gate.

© 2009 Elsevier Ltd. All rights reserved.

1. Introduction

The rapid growth of the mobile products market requires highly-integrated flash memories. Conventional flash memories, with a polycrystalline silicon layer as a floating gate, have been unable to satisfy the requirement for 10 years retention-time at low program/erase (P/E) voltage because of their nonscalability, particularly for the gate insulator thickness. Thus, a nonvolatile memory (NVM) consisting of discrete charge storage nodes with nanocrystals (NCs) was proposed as an alternative due to fast P/E speed and enhanced retention [1–4]. However, it has been difficult to obtain memory cell uniformity due to the random distribution of NCs. Also, there has been minimal research regarding theoretical analysis for the geometric effects of NC shape on NVM performance [5–7]. In this work, NVM memories with well-ordered and geometrically designed NCs of disc and cone shapes were fabricated and compared for the program efficiency of different NC shapes. Furthermore, analytical modeling was performed for the verification of NVM characteristics. Well-ordered NCs simplify and amplify the feasibility of the modeling. The consequences of this study

manifest that the program efficiency of NC-embedded NVM depends on the geometric shape of the NCs and the results will provide optimization for NC memory performance by controlling the shape of the NC.

2. Device fabrication

Fig. 1a shows a scanning electron microscope (SEM) image of a block copolymer (BCP) template with a 40 nm pore diameter and an 80 nm center-to-center distance. In this work, we applied cylinder-phase diblock copolymers composed of 70% polystyrene (PS) and 30% poly methyl-methacrylate (PMMA). A thin (80 nm) film of PS-*b*-PMMA was spin coated on neutrally treated Si wafer and annealed at 190 °C for 3 days. The resulting film with the PMMA cylinders perpendicular to the substrate was irradiated by ultraviolet rays ($\lambda = 254$ nm) and subsequently rinsed with acetic acid and with distilled and deionized water, and then dried in air. As a result, the cylinder-shaped cores of PMMA were removed and only the cross-lined PS matrix, which was an array of cylinder-shaped pores, remained. To remove residues inside the pores, oxygen plasma was used.

For the NVM fabrication, a p-type (100) wafer was used and a silicon insulator for 3-nm-thick tunneling dielectric was grown at 850 °C. A chromium (Cr) layer was evaporated onto the BCP template formed by the aforementioned procedure. The NC's height

* Corresponding author. Tel.: +82 42 350 5477; fax: +82 42 350 8565.

E-mail addresses: siege0@nobelab.kaist.ac.kr (S.-W. Ryu), ykchoi@ee.kaist.ac.kr (Y.-K. Choi).

¹ Tel.: +82 42 350 3477; fax: +82 42 350 8565.

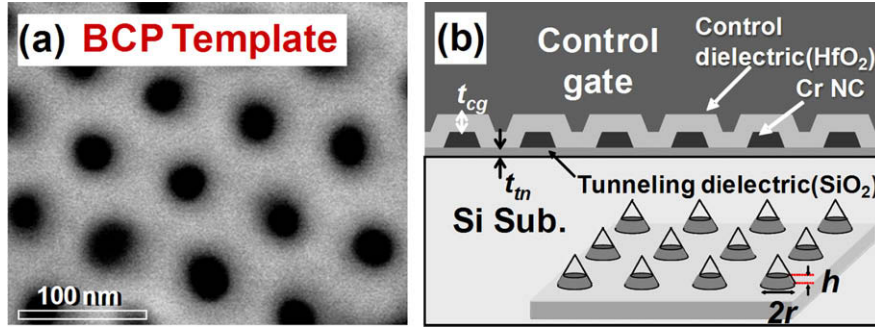


Fig. 1. (a) A SEM image of a BCP template with a 40 nm pore diameter and an 80 nm center-to-center distance, and (b) a schematic of NVM with designed Cr NC.

and shape were determined by controlling the evaporation time. By increasing the time, the shape was modulated from a disc to a cone due to the narrowed window of the pore because Cr was deposited more at the edge of the top and the sidewall of the BCP template than elsewhere. The BCP template and unwanted Cr layer were then removed by sonication process in toluene. After formation of Cr NCs, a 10-nm-thick hafnium oxide (HfO₂) as a control dielectric and a 300-nm-thick aluminum layer as a control gate electrode were deposited and defined.

3. Device modeling

Fig. 1b illustrates the schematic of the NVM with the designed Cr NC used for modeling. First, by considering the cone- and disc-shaped Gaussian surfaces according to NC shape, the electric field (*E*-field) in the control dielectric (*c_g*) and the tunneling dielectric (*t_n*) can be expressed as

$$E_{cg} = \frac{V_g}{t_{cg} + \frac{1}{k} \left(\frac{\epsilon_{hf}}{\epsilon_{ox}} \right) t_{tn}} + \frac{knq / (\pi r^2)}{\epsilon_{hf} + k\epsilon_{ox} \left(\frac{t_{cg}}{t_{tn}} \right)} \quad (1)$$

$$E_{tn} = \frac{V_g}{t_{tn} + k \left(\frac{\epsilon_{ox}}{\epsilon_{hf}} \right) t_{cg}} - \frac{knq / (\pi r^2)}{k\epsilon_{ox} + \epsilon_{hf} \left(\frac{t_{tn}}{t_{cg}} \right)} \quad (2)$$

where *V_g* is the gate voltage, ϵ_{ox} is the tunneling dielectric constant (SiO₂), ϵ_{hf} is the control dielectric constant (HfO₂), *t_{cg}* is the control dielectric thickness, *t_n* is the tunneling dielectric thickness, *r* is the NC radius, *k* is the NC surface area ratio, and *n* is the number of stored electrons in the NC. In Eqs. (1) and (2), *k* was defined as the surface area ratio of the NC in the tunneling dielectric over the surface area in the control dielectric, i.e. $k \approx \pi r^2 / \pi r^2 = 1$ for the disc-shaped and $k = \pi r^2 / \pi r \sqrt{r^2 + h^2}$ for the cone-shaped. This implies that the *E*-field in the tunneling dielectric is enhanced at a smaller *k*. Since the time interval for storing a single-electron in an NC is determined by the net current density (*J_{net}*) through the NC and *J_{net}* is a function of the electron number captured in the NC, programming time (*t_n*) for *n* electrons stored in the NC was calculated recursively with the relation of [8].

$$t_n = t_{n-1} + \frac{q}{\sigma J_{net}} \quad (3)$$

where σ is a capture area. In Eq. (3), *J_{net}* is the sum of the current density in the tunneling dielectric (*J_{tn}*) and the current density in the control dielectric (*J_{cg}*). Current density in the two oxide layers can be calculated by using the direct tunneling (DT) mechanism [9] or the Fowler–Nordheim (FN) tunneling mechanism according to its oxide energy band bending (Φ_{ox}) [10]. At this time, electron effective mass modulation was considered according to the *E*-field of each dielectric layer as expressed by [11].

$$m_{eff}^* = m_0^* (E_{eff} / E_0)^{2/3} \quad (4)$$

where *E₀* and *m₀^{*}* were the initial *E*-field and electron effective mass constants. Finally, the flatband voltage shift ($\Delta V_{fb} \propto \Delta V_{th} = nq / C_{cg}$) was obtained by considering all of the above equations with different *C_{cg}*s ($C_{cg_cone} = \epsilon_{hf} \pi r \sqrt{r^2 + h^2} / t_{cg}$, $C_{cg_disc} = \epsilon_{hf} \pi r^2 / t_{cg}$). In the modeling, the NC-to-NC lateral interference was assumed to be small due to a sufficiency of space (>30 nm) between NCs.

4. Device characteristics and discussion

Fig. 2a and b show SEM and atomic force microscopy (AFM) images of disc-shaped NCs (*r* = 15 nm, *h* = 5 nm) and cone-shaped NCs (*r* = 15 nm, *h* = 34 nm). As shown in Fig. 2, highly well-ordered NCs were obtained due to the uniform cores of BCP template. This ordering would be useful in achieving a desirable uniformity of NVM cells.

Fig. 3a and b show the high-frequency (1 MHz) capacitance–voltage (*C*–*V*) curves of NVM cells with disc-shaped NCs and cone-shaped NCs under the program voltage (*V_{G_PGM}*) of 6 V for different program times. After programming, ΔV_{fb} in the *C*–*V* plot represents that the NC formed by using the BCP mask layer served as a charge storage node of the NVM. Furthermore, the cone-shaped device has a better program efficiency (wider shift at the same program time) than the disc-shaped one. Ignoring the lateral interference NC-to-NC for the disc-shaped NC, the *E*-field parameter *k* is 1, and the capacitive-coupling ratio $C_{cg} / (C_{cg} + t_{tn})$ is 0.66. Considering the typical coupling ratio of conventional flash memory devices (0.5–0.6), the designed NVM with a disc-shaped NC shows similar performance. However, in the geometry of the cone shape, the C_{cg_cone} is much larger than the C_{cg_disc} . Thus, the coupling ratio of the cone-shaped NC is distinguishably increased to 0.83, which causes large voltage shift and *E*-field at the NC.

Fig. 4 shows the programming transient characteristics for both the disc- and cone-shaped NCs at *V_{G_PGM}* = 6 V and 8 V. Additionally, the measured data was verified and matched very well with the analytical modeling, as shown in Fig. 4. At *V_{G_PGM}* = 6 V and *t_{PGM}* = 1 s, ΔV_{fb} of the disc-shaped NC and cone-shaped NC are 1.5 V and 2.2 V, respectively. From the measured data, we find that the NVM with a cone-shaped NC works faster than the disc-shaped NC at the same *V_{G_PGM}* = 6 V. This is caused by the improved capacitive-coupling ratio. As discussed above, the large capacitive-coupling ratio induces a high *E*-field in the tunneling dielectric region, and then the flow of electrons in the cone-shaped NC is larger than in the disc-shaped NC. Hence faster change of ΔV_{fb} takes place in the cone-shaped NC. By contrast, at *V_{G_PGM}* = 8 V, ΔV_{fb} of the disc-shaped NC and cone-shaped NC are 2.6 V and 2.5 V. There is a crossover of the shift of flatband voltage between 1 ms and 10 ms. Up to 1 ms, ΔV_{fb} of the cone-shaped NC changes faster than that of the disc-shaped NC, which is due to the difference of magnitude of the *E*-field according to the NC shape and the capacitive-coupling ratio. Calculation data from the analytical model

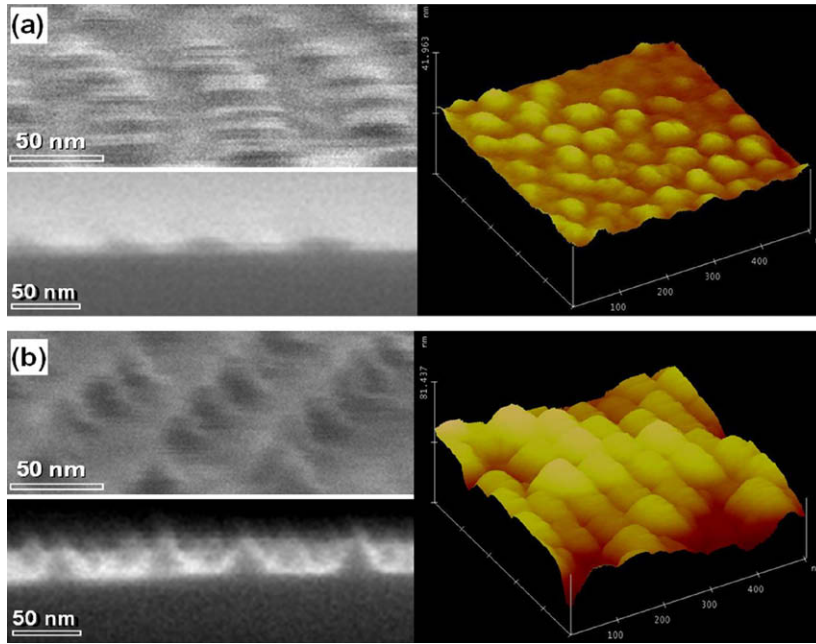


Fig. 2. SEM and AFM images of (a) disc-shaped NCs ($r = 15 \text{ nm}$, $h = 5 \text{ nm}$) and (b) cone-shaped NCs ($r = 15 \text{ nm}$, $h = 34 \text{ nm}$).

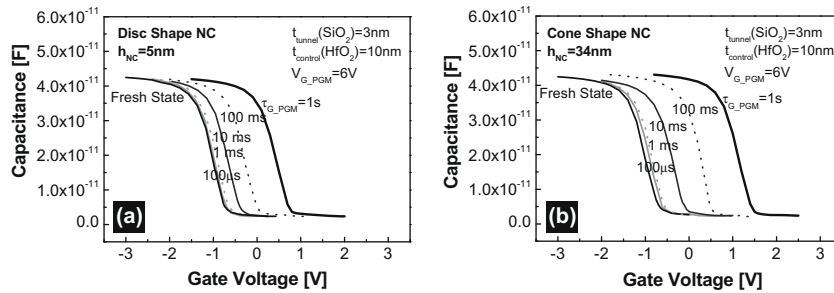


Fig. 3. High-frequency (1 MHz) C - V curves of devices with (a) disc-shaped NC and (b) cone-shaped NC at $V_{G_PGM} = 6 \text{ V}$ for different program times (100 μs , 1 ms, 10 ms, 100 ms, and 1 s).

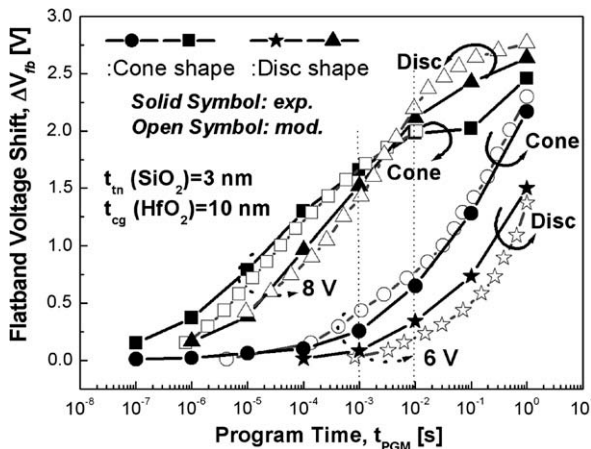


Fig. 4. The programming transient characteristics for both disc- and cone-shaped NCs. Both calculated and measured data are plotted and compared for $V_{G_PGM} = 6 \text{ V}$ and $V_{G_PGM} = 8 \text{ V}$.

show the initial E -fields in the tunneling dielectric for the disc-shaped NC and cone-shaped NC. The cone-shaped NC induces the larger initial E -field (17.4 MV/cm) than that of the disc-shaped

NC (14.8 MV/cm) in the tunneling dielectric due to the higher gate-capacitive-coupling-ratio. Thereby the cone-shaped NC-embedded device provides the larger tunneling current hence more electrons are stored in the NCs. Subsequently, it reduces E -field in the tunneling dielectric and in turn enhances E -field in the control oxide dielectric concurrently. Since the difference between J_{tn} and J_{cg} at the cone-shaped NC is more rapidly reduced than at the disc-shaped NC, $J_{tn} = J_{cg}$ condition is made earlier at the cone-shaped NC. It resulted in that after 1 ms ΔV_{fb} of the disc-shaped NC has a larger value than that of the cone-shaped NC. In short, for both 6 V and 8 V program voltages, the NVM with the cone-shaped NC has a better program efficiency than the NVM with the disc-shaped NC, in view of the fact that the large capacitive-coupling-ratio of the cone-shaped NC induces a large flow of electrons to the NC.

5. Conclusions

Geometric effects of NC shape on the memory characteristics in NVM have been investigated by comparing disc-shaped NCs and cone-shaped NCs. Using a BCP template, NVM with uniformly distributed and geometrically designed NCs was obtained. The modeled and measured data indicate that the program efficiency of a memory device depends on the geometric shape of its NC. A device

with a cone-shaped NC has a better program efficiency than that of a device with a disc-shaped NC due to the higher capacitive-coupling ratio. For both NC shape devices of disc and cone, retention characteristics were also measured. But they did not show any difference. Thus, it can be concluded that the enhanced program efficiency is achievable without sacrificing the retention characteristics by NC shape engineering.

Acknowledgment

This work was supported by the National Research Program for 0.1-Terabit Nonvolatile Memory Development, sponsored by the Ministry of Knowledge Economy, and was also supported by the Korea Science and Engineering Foundation (KOSEF) grant funded by the Korea government (MEST) (No. R0A-2008-000-20057-0).

References

- [1] Tiwari S, et al. Volatile and nonvolatile memories in silicon with nanocrystal storage. In: 1995 IEEE international electron devices meeting (IEDM), Washington, DC, USA; December 1995. p. 521–4.
- [2] Hanafi HI et al. Fast and long retention-time nanocrystal memory. *IEEE Trans Electron Dev* 1996;43:1553–8.
- [3] Tiwari S et al. Small silicon memories: confinement, single-electron, and interface state considerations. *Appl Phys Lett* 2000;71:403–14.
- [4] Chen JH et al. Nonvolatile flash memory device using Ge nanocrystals embedded in HfAlO high-*k* tunneling and control oxides: device fabrication and electrical performance. *IEEE Trans Electron Dev* 2004;51:1840–8.
- [5] Carreras J et al. Dynamical modeling of transport in MOS structures containing silicon nanocrystals for memory applications. *Microelectron Eng* 2008;85:2378–81.
- [6] Sousa JS et al. Three-dimensional self-consistent simulation of the charging time response in silicon nanocrystal flash memories. *J Appl Phys* 2002;92:6182–7.
- [7] Sousa JS et al. Effects of crystallographic orientations on the charging time in silicon nanocrystal flash memories. *Appl Phys Lett* 2003;82:2685–7.
- [8] Hou TH et al. Design optimization of metal nanocrystal memory –Part I: Nanocrystal array engineering. *IEEE Electron Dev Lett* 2006;53:3095–102.
- [9] Yeo YC et al. Direct tunneling gate leakage current in transistors with ultrathin silicon nitride gate dielectric. *IEEE Electron Dev Lett* 2000;21:540–2.
- [10] Lee WC. Modeling CMOS tunneling currents through ultrathin gate oxide due to conduction- and valence-band electron and hole tunneling. *IEEE Trans Electron Dev* 2001;48:1366–73.
- [11] Sze SM. *Physics of semiconductor devices*. New York: Wiley-Interscience; 2007.